Evolution of the Glorieuses seamount in the SW Indian Ocean and surrounding deep Somali Basin since the Cretaceous

E. Leroux, J. Counts, S. Jorry, Gwenael Jouet, S. Revillon, M.K. K Boudagher-Fadel, S. Courgeon, C. Berthod, Gilles Ruffet, Patrick Bachèlery, et al.

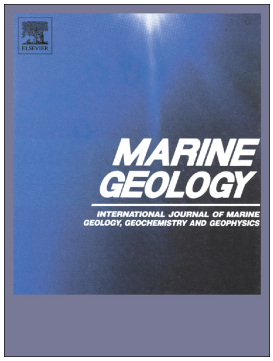

Evolution of the Glorieuses seamount in the SW Indian Ocean and surrounding deep Somali Basin since the Cretaceous

E. Leroux, J. Counts, S. Jorry, G. Jouet, S. Révillon, M.K. BouDagher-Fadel, S. Courgeon, C. Berthod, G. Ruffet, P. Bachèlery, E. Grenard-Grand

PII: S0025-3227(20)30090-6

DOI: https://doi.org/10.1016/j.margeo.2020.106202

Reference: MARGO 106202

To appear in: *Marine Geology*

Received date: 11 December 2019

Revised date: 6 April 2020

Accepted date: 8 April 2020

Please cite this article as: E. Leroux, J. Counts, S. Jorry, et al., Evolution of the Glorieuses seamount in the SW Indian Ocean and surrounding deep Somali Basin since the Cretaceous, *Marine Geology* (2020), https://doi.org/10.1016/j.margeo.2020.106202

EVOLUTION OF THE GLORIEUSES SEAMOUNT IN THE SW INDIAN OCEAN AND SURROUNDING DEEP SOMALI BASIN SINCE THE CRETACEOUS

E. Leroux (1), J. Counts (2), S. Jorry (1), G. Jouet (1), S. Révillon (3), M.K. BouDagher-Fadel (4), S. Courgeon (1,5), C. Berthod (6), G. Ruffet (7), P. Bachèlery (6), & E. Grenard-Grand (1,8)*

(1) IFREMER, Laboratoire Géodynamique et enregistrements Sédimentaires, BP70, 29280 Plouzané, France
(2) University College Dublin, School of Earth Sciences, Belfield, Dublin 4, Ireland
(3) SEDISOR, Place Nicolas Copernic, 19280 Plouzané, France
(4) University College London, Department of Earth Science, London, United Kingdom
(5) University of Genève, Department of Earth and Environmental Science, 13 Rue des Maraîchers, Geneva, Switzerland
(6) Université Clermont-Auvergne, UCA-OPGC, Laboratoire Magma et volcans, 4 avenue Blaise Pascal, 63178 Aubière cedex, France
(7) Université de Rennes 1, Géosciences-Rennes, UMR 6118, Campus Beaulieu, 35042 Rennes cedex, France
(8) Université de Caen-Normandie, UMR 6143 M2C morphodynamique continentale et côtière, 24, rue des Tilleuls, 14000 Caen cedex, France.

**corresponding author: estelle.leroux@ifremer.fr*

ABSTRACT (380 words)

Little is known about the geological history of the Glorieuses seamount including basic information about its age and origin related to the regional evolution of the southern tip of the Somali Basin. This study focused on describing and reconstructing the long-term stratigraphic evolution of the Glorieuses seamount (SW Indian Ocean) to identify the mechanisms that have occurred through time to finally shape the emerged modern islands. Distinct terrace levels, currently submerged along the flanks of the seamount and surrounding seamounts, have already been interpreted as resulting from successive carbonate development and back-stepping episodes over the last 62 Myr. New isotopic and biostratigraphic dating on the flanks of the seamount, coupled with sequence stratigraphic interpretation of seismic profiles acquired in the adjacent basin, provide new constraints for the Late Cretaceous and Cenozoic vertical evolution of the seamount topped by carbonate platforms and sedimentation in the surrounding deep basin. Even if starved steep slopes prevent a straightforward source-to-sink continuity between the platform and the basin domains, our findings propose a consistent chronostratigraphic framework for the identified seismic markers and sequences in the deep

basin, and discuss a long-term geological model that includes the main driving factors behind deposition (volcanic events, subsidence vs uplift phases, climate and hydro-dynamism changes) and their quantitative impact on the evolution of the isolated carbonate sedimentary system. Our results show that: (i) the Glorieuses volcanic seamount emerged from two successive Late Cretaceous magmatic pulses, firstly during the Turonian, then during the Maastrichtian (ii) at least two potential uplift phases are recognized during the Tertiary (Paleogene and/or the Eocene and Tortonian); (iii) basinal sedimentation recorded an abrupt change probably related to major regional hydro-dynamical changes in Late Eocene times in the Western Indian Ocean; (iv) the export of sediments from the platform towards the basin (numerous gravity flow processes) is strongly enhanced after the Mid Miocene, and is probably linked to the onset of the Asian monsoon winds and bipolar circulation. Finally, the Glorieuses seamount, although located in the vicinity of the Comoros islands, appears to have a much longer history and is geologically more comparable to the nearby Seychelles. This long-term study has enabled us to associate the Glorieuses seamount with the SSE-NNW Madagascar-Seychelles alignment rather than with the Comoro hot spot evolution.

Key words: *Glorieuses seamount, Somali Basin, seismic stratigraphy, tectonics, vertical movement (uplift and subsidence), volcanism, shallow-water carbonate platform,* $^{40}Ar/^{39}Ar$.

1. INTRODUCTION

Darwin's canonical model of reef development (Darwin, 1842) proposes an evolutionary sequence of reef formation as a volcanic island ages and subsides, from fringing reef to lagoon-bounding barrier reef to atoll. However, many islands do not follow this sequence, and few modern environments have the right combination of conditions (island subsidence, coral growth, and sea-level variations) to produce the Darwinian atoll progression (Toomey et al., 2013). The Mozambique Channel (South West Indian Ocean - Figure 1) is characterized by scattered and steep-sloped seamounts that host shallow-water carbonate platforms and coral reefs called the Eparses Islands (Battistini and Cremer, 1972; Battistini et al., 1976a; Battistini et al., 1976b; Maugé et al., 1982, Guillaume et al., 2012; Jorry et al., 2016; Counts et al., 2018). The Eparse Islands include the Glorieuses Archipelago located ~200 km north of Madagascar in the southern tips of the West Somali Basin. The Glorieuses Archipelago is composed of one main edifice emerging at the location of two main islands (the Grande Glorieuses and the Lys Islands -Figure 1) with scattered fossil outcrops (Andréfouët et al. 2008) extending over 17 km in a NE–SW direction.

Little is known about the geological history of these seamounts, including basic information about their age and origin. These islands have been considered to represent (i) an early section of a volcanic track generated by the Comoros hot spot (Emerick and Duncan 1982, but see Courtillot et al. 2003) or (ii) synchronous magmatism along inherited lithospheric fractures trending NNW, from northern Madagascar onto the islands of the Seychelles Aldabra group (Nougier et al., 1986).

This paper explores the long-term evolution of the Glorieuses islands to identify (and quantify) the mechanisms that have shaped the islands. It also provides a detailed assessment of regional stratigraphy to clarify the geological relationship between islands in the southern Somali Basin.

Our approach also ties our observations and results on the long-term evolution of the Glorieuses seamount to previous offshore investigations of the deep-water areas offshore/onshore northern Mozambique to discuss and highlight possible regional correlative events.

2. GEOLOGICAL SETTING

2.1. TECTONIC FRAMEWORK OF THE MOZAMBIQUE CHANNEL

As summarised by Castelino et al., (2015) the separation of East and West Gondwana resulted in the formation of extensional sedimentary basins along the African margin (Jokat et al., 2003; Koenig and Jokat, 2010; Mahanjane, 2012; Nairn et al., 1991; Reeves, 2000; Salman and Abdula, 1995). The break-up of Gondwana (Figure 2) has been described as a two-phase process (Cox, 1992; Eagles and König, 2008; Leinweber and Jokat, 2011; Mahanjane, 2012; Reeves, 2000). The seafloor spreading record in the Mozambique Basin can be simply interpreted in terms of the divergence of Africa and Antarctica. Considering a fixed Africa, initial rifting in Early Jurassic times occurred in response to a southwest-directed motion of Antarctica. This displacement was followed by southward relative movement during the second phase. Prior to the onset of continental break-up, Madagascar was located in central Gondwana, adjacent to the present-day Tanzania, Kenya, and Somalia margins. Although a subject of debate for a long time (Flores, 1984; Foerster, 1975; Kamen-Kaye, 1982), it is now widely accepted that Madagascar drifted southwards from Tanzania along the Davie shear zone (Rabinowitz et al., 1983; Coffin and Rabinowitz, 1987) or the Davie Ridge Transform fault system. During its drift phase, Madagascar moved southwards during the Early Cretaceous (Davies et al., 2016) probably from M0r (Müller and Jokat, 2019). The island has occupied its present position as part of the African plate since the termination of seafloor spreading in the West Somali Basin (Cochran, 1988; Eagles and König, 2008; Rabinowitz et al., 1983; Salman and Abdula, 1995). Although detailed kinematic reconstructions need to be more accurately modelled for the whole separation of East and west Gondwana (Reeves, 2014 ; Phetean et al, 2016 ; Davis et al., 2016 ; Thompson et al., 2019, Müller and Jokat, 2019) and subsequent crustal structures better refined and delineated in the Mozambique channel (e.g. Klimke & Franke, 2016, Müller and Jokat, 2019), this rough configuration results in a fairly simplified structural setting: northeastern Kenya/Somalia and northern Madagascar resemble conjugate passive rift margins, whereas southeastern Kenya/Tanzania/northern Mozambique and western Madagascar are conjugate transform margins (Coffin and Rabinowitz, 1992). Figure 1 indicates the geological basins (Rovuma,

Morondava, Ambilobe, Majunga…) that subsequently separated following the key stages in the separation of Madagascar from its neighbours in Gondwana (Figure 2).

2.2. STRATIGRAPHIC FRAMEWORK

Seafloor spreading ceased in the West Somali Basin in the Early Cretaceous (Coffin and Rabinowitz, 1992). It has been consistently reported that a passive margin sedimentary system exists since the beginning of the Late Cretaceous in the West Somali Basin (Key et al., 2008; Nicholas et al., 2007). In the northern Mozambique Basin, West of Davie Ridge, the upper parts of the post-break-up successions have been drilled, providing stratigraphic control on the seismic marker horizons: the Neocomian Unconformity, the Top Cretaceous/Base Tertiary, and the Pliocene Unconformity (Mahanjane et al., 2014). Results of commercial exploration of the Rovuma Basin also provide a relatively well-defined Late Mesozoic to recent stratigraphy in northern Mozambique (e.g., Key et al., 2008; Nicholas et al., 2007; Salman and Abdula, 1995).

In the west Somali Basin, some Glorieuses fossil coral reefs have been studied (Battistini et al., 1976a, 1976b; Gaven and Vernier, 1979; Guillaume et al., 2013; Jorry et al., 2016, Prat et al., 2016 Counts et al., 2018), but until now, most of the attention was focused on the platform over the last climatic cycles at Pleistocene scale (Jorry et al., 2016, Counts et al., 2018); the stratigraphy of Glorieuses seamount thus remains barely constrained at longer time-scales. An absolute age measured with Strontium Isotopic Stratigraphy (SIS) from a dredged sample on a terrace (750 m deep) provided a single stratigraphic constraint: the record of this Selandian to Thanetian (~62 Ma) terrace, composed of shallow-water carbonates, implies that the main volcanic event responsible for the formation of the seamount occurred before the Late Paleocene (Courgeon et al., 2016). Ages of the oceanic crust in the Western Somali Basin extend from Middle Jurassic to Upper Cretaceous, between 165 and 130 Ma (Rabinowitz et al., 1983; Kent and Gradstein, 1985). Thus, at this stage, we can only roughly estimate that the Glorieuses seamount reached the photic zone between 130 Ma and 62 Ma.

The occurrence of a deeper terrace at approximately 1100 m deep, also assumed to be carbonated, suggests that carbonate production started even before the Late Paleocene, i.e., most likely during Early Paleocene or Late Cretaceous (considering a simple continuous subsidence of the seamount over its history). Overall, the distinct terrace levels observed along the flanks of the Glorieuses edifice are interpreted as resulting from successive carbonate platform development and backstepping episodes, prior to the initiation of the modern carbonate system (Courgeon et al., 2016).

The Glorieuses platform does not exhibit evidence of major drowning events during its Cenozoic development. Moreover, no evidence of tectonic nor of any renewed volcanic activity has been observed along its flank or in the proximal basin, suggesting that the Glorieuses carbonate platform has evolved in an overall stable geodynamical setting since Early Paleogene times. Taking into account that Paleocene eustatic sea level was approximately 50 m above present day sea level (Miller et al., 2005), the average

subsidence of the Glorieuses seamount since the Paleocene is estimated between 10 and 15 m. Myr^{-1} (Courgeon et al., 2016).

2.3. MAGMATISM/VOLCANISM IN THE NORTHERN MOZAMBIQUE CHANNEL

Within the geodynamic evolution and breakup of Gondwana including Indian Ocean opening, extensive volcanism has been recorded in the study area on onshore Madagascar, with a large trapp formation during Turonian times (Storey et al., 1995) and volcanic episodes associated with the reactivation of ancient structures during the Paleogene (Rasamimanana et al.,1998). The Late Jurassic ocean crust (Tithonian ~150 Ma; Müller et al., 2008) in the Somali/Comores Basin and Mozambique Basin was penetrated by extrusive volcanic edifices from the Early Cenozoic to modern times (Bardintzeff et al., 2010; Class et al., 1998; Emerick and Duncan, 1982). These volcanic edifices crop out in the Comoro Islands (from East to West: Mayotte, Anjouan, Mohéli and Grande Comore), and have resulted in reef development at Geyser-Zélée and Leven banks and at Glorieuses, as well as Juan de Nova, Europa and Bassas da India islands in the southwards Mozambique channel, but also at the Aldabra, Assumption, Cosmoledo and Astove groups, the Farquhar and Providence groups in the North (Figure 1). Initiation, nature and age of the volcanism of all these edifices are still poorly known or incompletely understood. The progressive westward decreasing ages of volcanism from Seychelles-northern Madagascar-Mayotte-to Grande Comoro is classically attributed to a hot spot tracked from the Seychelles Plateau to the Grande Comore (Emerick and Duncan, 1982). But this was questioned by Nougier et al. (2006) who suggested an alternate interpretation that involves a more or less synchronous alkaline magmatism along inherited lithospheric fractures (from Madagascar continent toward Comoro oceanic islands), periodically reactivated during Tertiary times. Geochronological data seems to corroborate the diachronous magmatic activity, starting in Mayotte at least 10.58 Ma ago, in Mohéli and Anjouan around 3.9 and 5 Ma, respectively, and finally in Grande Comore since 0.13 Ma (Hajash and Armstrong, 1972; Emerick and Duncan, 1982, 1983; Nougier et al., 1986; Debeuf, 2004; Pelleter et al., 2014). It is worth noting that a syenite xenolith dated at 11.1 Ma in Anjouan (Montaggioni and Nougier 1981; Nougier et al. 1986) suggests an early phase of magmatic activity coeval with Mayotte volcanism (Nougier et al. 1986). For Mayotte, a maximum age of 15 Ma was first estimated for the onset of the magmatic activity on the seafloor (−3300 below sea level) (Nougier et al. 1986), earlier than suggested by Michon (2016). By combining realistic magma production rates, volume of each edifice and geochronology, the author estimates that magmatic activity started first in Mayotte about 20 Ma ago and secondly, almost simultaneously, in Anjouan, Mohéli and Grande Comore about 10 Ma ago.

Within Seychelles archipelago, according to Plummer (1995), five important igneous events are recorded since the Cretaceous : (i) basic dykes at 135 Ma, that are temporally equivalent to the Marion hotspot-related Lebombo and Movene volcanics of South Africa and Mozambique; (*ii)* igneous interbeds at 124-113 Ma possibly correlated to the Marion hotspot; *(iii)* tholeiitic basalts of the Amirante Ridge

complex at 82-?65 Ma ; (*iv)* the Deccan event at ~70-60 Ma divisible into pre-Deccan tholeiitic (~70-68 Ma), main Deccan basic (-68-63 Ma) and post-Deccan acidic magmatism (-63-60 Ma); and *(v)* basalts extruded at ~47 Ma when the drift of SeychelIes/Mascarene coincided with the Deccan-Reunion hotspot at Saya de Mahla. Acid volcanics from the northeast coast of Madagascar, and offshore the Indian west coast are also related to the beginning (~96 Ma) and end (~84 Ma) of rifting between Seychelles/India and Madagascar.

3. DATA AND METHODS

This study focused on Glorieuses area and the surrounding basins and further southward to the Majunga Basin (Figure 1). It mainly relies on the 2014 PTOLEMEE (PasT GlObaL ChangEs in the MozambiquE channEl) high resolution seismic survey (Jorry, 2014). Multichannel (24 traces) seismic acquisition was done at high-speed (acquisition at 10 knots) with airgun-sourced. This seismic dataset includes 31 profiles acquired all around the Glorieuses archipelago with a line spacing of ~ 10 km for a total length of ~900 km as shown in Figure 1b (dotted black lines); it includes also 8 profiles of ~300 km southwestward (Figure 1, pink straight lines) until the Majunga margin ~300 km away. Another seismic multichannel line from ION (Figure 1, black straight line) allowed us to image the sediment infilling from the Majunga margin (SE) to Mayotte island (NW) along a 250 km transect.

Principles of seismic and sequence stratigraphy were used to interpret this dataset (Mitchum et al., 1977). This study is also based on five dredges made on the flanks of the Glorieuses archipelago during the Biomaglo cruise (Corbari et al., 2017) (Figure 1), providing stratigraphic constraints in terms of environment and age, as well as clues for the amplitude of vertical movements. Stratigraphic data are based on planktonic and benthic foraminifera biostratigraphy (BouDagher-Fadel, 2015, 2018a, b) and strontium isotopic stratigraphy (SIS; McArthur et al., 2012). In our definitions of stratigraphic ranges, we primarily use the Planktonic Foraminifera zonal scheme of BouDagher-Fadel (2015, 2018b), which is tied to the time scale of Gradstein et al. (2012) and revised by Cohen et al. (2017).

This study also relies on petrological analyses and $^{40}Ar/^{39}Ar$ dating from another dredge (DR04) performed on the NW-SE Ridge, in the north-western part of the Glorieuses volcanic edifice (Figure 1b) during the 2014 PAMELA-MOZ01 cruise (Olu, 2014). Analytical data and parameters used for calculations (e.g. isotopic ratios measured on pure K, Ca and Cl salts; mass discrimination; atmospheric argon ratios; J parameter; decay constants) and reference sources are available in the Supplementary Material 2 for details.

Time-depth conversions of seismic lines used a mean acoustic velocity of 2 km/s in order to provide a first approximation for rough sediment thickness. This value is averaged from DSDP Reports for wells 240–242 and Marion Dufresne seismic profiles in the Comoro Sea that show velocities from 1.5–2.92 km/s (Simpson et al., 1974; Lort et al., 1979). Note here that these volumes correspond to rough estimates calculated with a mean velocity for the entire sediment column, and are not corrected for

porosity. These estimates must therefore be taken with caution, and are only useful here to provide a first order quantitative assessment of volumetric distribution between sequences.

4. RESULTS

4.1. SEISMIC STRATIGRAPHY

Seismic lines acquired on the lower slopes and proximal basins adjacent to the Glorieuses platform show several distinct types of sedimentary deposits, which can be classified based on the amplitude, continuity, and orientation of their internal reflections.

First, seismic facies can be organised into three regional sequences (Figures 3, 4, 5, 6, 7) at the toe of slope and in the deep basin above the acoustic basement (grey): S1 (green), S2 (red), and S3 (yellow). Sub-units (a, b) are also identified within S1, S2 and S3. These three regional sequences can be recognized on both (leeward -Figures 3- and windward -Figure 4) sides of the seamount (Figure 6).

S1 is characterized by a universally transparent seismic facies and an aggradational geometry of very weak amplitude. Reflection spacing is unchanged within the entire column, and reflections display little or no internal structure, which is an indication for continuous sedimentation of similar material over the represented period of deposition. Occasionally, very high amplitude reflections (bright spot) can be observed locally, interpreted as volcanic sills. Within the upper part of S1 (called S1b), we observe less transparent, slightly deformed but more chaotic facies than within S1a (Figures 5, 6). S1 is bounded at its top by a regional high amplitude, continuous reflection (green horizon on Figure 5).

The two successive sequences S2 & S3 show many lateral facies changes in contrast to S1. The overlying S2 sequence is characterized by moderate to high amplitude, parallel or sub-parallel reflections (Figure 4) which locally show onlap geometries in their lower part, sub-unit 2a. These are interpreted here as an occurrence of erosional discontinuities shaped by bottom currents.

Finally, the S3 sequence is differentiated from S2 because of a change towards a more transparent seismic facies, and an increase in lateral facies changes, due in particular to the many observed erosive features (larger reworked depositional features -Figure 4, channel incision -Figure 5). The appearance of S3 is variable, but a thin transparent superficial layer (figure 4), sometimes associated with wavy bedforms, is clearly imaged.

As previously described by Counts et al (2018), superficial sedimentary features (10-15 m below seafloor) in the lower slope and proximal basin (2000–3500m deep) consist of basin floor pelagites/hemipelagites, channels, levees, and turbidites lobes, and mass transport deposits (MTDs) (Figures 3, 4, 5)**.** Locally, seismic morphologies and facies also evidence volcanic domes, occasionally reaching seafloor (Figure 3). Steep slopes of the Glorieuses seamount preclude thick sedimentary sequences whereas slope display both erosive (incised valley, paleo-channel, scarps) and depositional features (channel infill, MTD – Figure 4). An elongated contourite drift (Faugeres and Stow, 1993),

directly overlying the basement at depth around 5.6 s TWTT (within S1, or S2), also appears on the leeward side of the seamount (Figure 4). Its length reaches almost 10 km while its height is roughly estimated to (at least) 250 m (v=2000 m/s). Its strongly eroded top suggests highly energetic erosive processes at the transition between S1 and S2. In general, S2 thus seems to represent a regional transition from undisturbed sedimentation (S1) to drift-altered deposition, and the beginning of Mass-Transport Deposition (S3).

Underlying the entire sequence, we can also locally identify a S0 unit characterized by mixed amplitude chaotic reflection within the basement lows (dark green on Figure 3). This unit possibly represents volcanoclastic deposits just after the volcanic edification of the basement.

4.2. AGE DATING OF DREDGE ROCKS

Several dredging operations have been conducted along the flanks and terraces of the Glorieuses seamount. DR04-10 and DR04-11 dated samples (location in Figure 1) display sub-alkaline composition and belong to a differentiated series ranging from benmoreites to trachytes. SiO_2 and Na_2O+K_2O contents vary between 53.69 – 58.45 wt.% and 7.93 – 10.87 wt.%, respectively (Supplementary Material 3). Content of K_2O ranges from 2.88 to 4.02 wt.% allow us to performed $^{40}Ar/^{39}Ar$ dating on whole rock single grains.

Textures and mineral assemblages are presented Figure 8. DR04-10 sample is characterized by a microlitic texture (Figure 8a). The microlitic groundmass contains 50 – 300 µm plagioclase laths and cubic 10 – 100 µmFe-Ti oxides. DR04-11 sample present porphyritic texture with 500 µm – 3 mm plagioclases and few 500 µm – 1 mm pyroxene macrocrysts (Figure 8b). Groundmass have a microlitic texture and contains100 – 500 µm plagioclase laths, 50 – 200 µmFe-Ti oxides and scarce apatite and sphene microcrystals. It is worth nothing that these parageneses are consistent with sub-alkaline compositions.

Since they represent the first volcanic rocks obtained for the submarine section, dredged rocks constitute an important material to date the Glorieuses archipelago volcanism.

The two samples DR04-10 and DR04-11 provide age spectra with fairly similar shapes, with high ages in the low temperature steps (0-10% of 39Ar degassed) and a decrease in apparent ages in the high temperature steps. This shape of the age spectra reflects a fairly significant alteration/weathering of the analyzed grains. The shape of the DR04-10 age spectrum, more pronounced than that of the DR04-11 sample, suggests that it is more altered/weathered. This seems to have to be compared with their respective $^{37}Ar_{Ca}/^{39}Ar_K$ spectra (# Ca/K), which are in a ratio of 2.5 to 3. The $^{37}Ar_{Ca}/^{39}Ar_K$ spectrum of the DR04-10 sample suggests that this material is more calcic and/or less potassic than that of the DR04-11 sample. This could either express a more significant alteration/weathering of DR04-10 or indicate that

the material is more likely to be altered/weathered. These observations are consistent with the convergence that can be observed between the two age spectra at intermediate temperature steps. This convergence tends to validate the pseudo-plateau age at 69.5 ± 0.1 Ma (72.8% of 39ArK released) yielded by DR04-11 sample, the apparently least altered/weathered material. This age is perfectly confirmed by analysis in an inverse isochron diagram (correlation diagram) ($^{36}Ar/^{40}Ar$ vs. $^{39}Ar_K/^{40}Ar^*$; Turner, 1971; Roddick *et al*., 1980; Hanes *et al*., 1985) with a ratio ($^{40}Ar/^{36}Ar$) indistinguishable from the atmospheric ratio ($^{40}Ar/^{36}Ar$= 298.56 according to Lee et al. (2006)) and an MSWD of 1.01 in accordance with the statistical validity criteria (Figure 8c, and see Supplementary Material 3).

4.3. BIOSTRATIGRAPHY

Results of isotopic and bio-stratigraphic analyses on carbonate samples from 7 dredges are synthetized in Table 1 and Figure 9a,

Note that bathymetric estimates (according to foraminifera's observations, see Table 1) consider (i) the inner neritic zone at depths between low tide level and 30 m, (ii) the outer neritic zone at depths between 100 m and approximately the edge of the continental shelf or between 100 and 200 m, and (iii) the shallow-water reef at water depth ranging between 10 and 30 m associated to low to moderate energy. Biostratigraphic analysis indicate that DW4819A/B and DW4814A/B are wackestone of inner neritic planktonic foraminifera assemblages with reworked Early to Middle Miocene shallow reefal larger benthic foraminifera (e.g. *Alveolinella praequoyi,* - Supplementary Material 4A). The presence of *Globoquadrina dehiscens* (Supplementary Material 4B), *Globorotalia merotumida* (Supplementary Material 4C), *Prosphaeroidinella disjuncta* (Supplementary Material 4D), *Sphaeroidinellopsis subdehiscens* (Supplementary Material 4E), *Globorotalia praemenardii* (Supplementary Material 4F), *Orbulina universa* (Supplementary Material 4G), *Pulleniatina primalis* (Supplementary Material 4H), *Dentoglobigerina altispira* (Supplementary Material 4I) indicates a Late Miocene age, N16b-N18, 9-5.3Ma. For DW4815A/B, a micritic packstone of larger benthic foraminifera and algae where sparite has replaced micrite in many places. The larger benthic foraminifera include *Borelis* sp. (Supplementary Material 4J) and *Discocyclina* sp. (Supplementary Material 4K). These foraminifera and rare planktonic foraminifera such as *Paragloborotalia nana* confirm a Late Eocene age, P15-P17, 38-33.9Ma. Common algae such as *Distichoplax biseralis* and *Halimeda* spp. are also present. These assemblages indicate the deposition occurred in shallow water reefal environment with low to moderate energy.

5. INTERPRETATION

5.1. RELATIVE AGE ESTIMATE OF THE GLORIEUSES SEAMOUNT

No chronostratigraphic data is available for the deep basin. In this section, we attempt to correlate the seismic sequences and units observed in the Glorieuses deep basin to the southern and western

sediment records, in order to connect the area with well-established stratigraphic and geochronologic constraints in better known adjacent basins.

Seismic profiles on Figures 7a, 7b, 7c (location in Figure 1) image sediments in the West Somali Basin, infilling from the Glorieuses Seamount (in the North) to the Majunga Margin (in the South), and crossing through Mayotte Island (westwards). These profiles provide evidence for the relative chronostratigraphy of the volcanic edifices in the area, i.e. Glorieuses, Geyser-Zélée and Mayotte, and allow the sequences and sub-unit boundaries (bases of S1a, S1b, S2, S3) identified in the Glorieuses surrounding basin to be extended. These sequences do not necessarily correspond to different lithological units, but rather to chronostratigraphic units, and are henceforth referred to as "Age Units (AU)" rather than "units" to avoid any confusion.

Chrono-stratigraphic correlations along the seismic lines indicated on Figure 1 (black lines) allowed us to follow the identified chrono-horizon (tops of S1a, S1b, S2a, S2b) from the seismic lines in the basin surrounding Glorieuses seamount (Northernmost area) until the seismic lines in front of Saint-André Cape, Southward (location in Figure 1). The age model in this area was already established from seismic markers identified by Delaunay (2018) and calibrated on the Chesterfield borehole (location in Figure 1). It thus let us attribute ages for some of our geological time series in particular for the base of S1 (Turonian age), and the top of S1a (K/T boundary) (Figures 7). Figure 7b is a NNW-SSE line-drawing from Mayotte Island to the Majunga margin. Two traced reflectors, R1 (purple in Figure 6b) and R2 (light green in Figure 7b) correspond to the respective top of the Turonian volcanism and the Cretaceous/Tertiary limit after correlation to Chesterfield (location on Figure 1) well data (Delaunay, 2018; Grenard-Grand, 2018; Pers. comm. Dall'Asta M., 2019).

The base and the top of the main volcanic edifice of Geyser bank are respectively picked in light brown (Base VoG) and orange (Top VoG) (Figure 7a). This clearly shows that the top of the Glorieuses volcanic basement (Top of Turonian volcanism in purple) corresponding to the base of AU-S1a (dark green) is much deeper than the volcanic edification of the Geyser Zélée banks (between Base VoG and Top VoG reflectors within AU-S2 in light red). It thus appears that Glorieuses seamount is much older than Geyser/Zélée. The base of the Geyser seamount also corresponds (more or less) to the top of the AU-S1b.

It thus appears that: (i) the base of AU-S1a unit, i.e. the top of the Glorieuses volcanic basement, corresponds to the Top of the Turonian volcanism (~93-90 Ma); (ii) the top of AU-S1a is correlated to the Cretaceous/Tertiary Limit (~65 Ma); (iii) the main volcanic edification phase in Mayotte occurred above the top of S1b unit, within AU-S2. As for Geyser, Mayotte edification is much younger than Glorieuses; moreover, main volcanism in Mayotte seems to occur after the event forming the Geyser-Zélée banks, after the top of AU-S1b.

Picking the base and the top of a chaotic/transparent seismic facies (Figure 7b) allowed us to delineate the top and the base of the main phase of volcanic activity of Mayotte, whose ages range from

~15-20 Ma to ~3 Ma according to several authors (Nougier et al., 1986, Pelleter et al., 2014, and Michon, 2016). These ages provide us rough chronostratigraphic constrains within AU-S2 & AU-S3; unfortunately, we were not able to pick the top of AU-S2 and are therefore unable to decipher if the volcanic edification of Mayotte occurred simultaneously with the deposit of the S2 or S3 sequences around Glorieuses.

We can also note that sediment infill on the Transkei Basin in the South-West of the Mozambique channel (Schlüter & Uenzelmann-Neben, 2007) displays a stacked pattern of seismic facies surprisingly similar to the sequences identified in this study, particularly for S1a, S1b sequences and for transition to S2 & S3 sequences (Figure 6). Ages attributed by these authors are also fully consistent with our age model in our study area. These two regions are very far away from each other, but the K-T boundary is a world-wide event (associated with huge volcanism). Thus, it wouldn't be a surprise that this event could have left a similar imprint (volcanic ash dispersal, climate change … for instance) onto even distant stratigraphic records. The well-marked transition between the other identified main sequences (S1/S2 and S2/S3) could also be related to regional (volcanic-tectonic phases) and/or world-wide events (climate change). We will discuss this further in the discussion.

5.2 SEDIMENT THICKNESS MAPS

Figure 10 highlights qualitative and quantitative sediment dynamics through time. Figure 10a shows, from top to bottom, the isochron maps of the respective tops of the acoustic basement, and the tops of sequences S1 and S2 as identified on the lower slope and in the deep basin. The rather homogenous depth of the area to the top of the acoustic basement (~93-90 Ma) differs on the East (present-day windward side) compared to the West (leeward side) sides of the platform at the top of S1. This trend remains until today (Figures 10a & present-day bathymetric map in Figure 1b), with the exception of the southernmost part of the windward side, which underwent a relative shallowing between S1 et S2 deposits. It also appears that a channel, located East of the Glorieuses platform, is incised within S3 sequence.

Figure 10b displays, from top to bottom, the thickness maps of sequences S1 to S3 (increasing age order), and estimates of their respective volumes (Table 2). Qualitatively, sediment thickness appears homogenous and similar on the leeward and windward sides of the platform during S1, whereas a depocenter is clearly imaged on the East side of the seamount during S2. We can also infer that the time of S2 deposition is characterized by a strong sediment influx from the SE, whose thickness progressively decreases north and westwards. It includes the Mass Transport Deposit identified on seismic (Figure 4) that likely originates from the north of Madagascar. During S3, sediment thickness in the surrounding basin appears homogenous between the East and West, but in detail, alternating areas

of non-deposition and deposition at the toe of slope indicate several discrete pathways for sediments that are exported from the Glorieuses platform. This process may become more prominent in S3, particularly on the west side (leeward side) where an adjacent depocenter appears in a more proximal location relative to the East. Differences in sediment transfer from platform to basin between East and West may be also linked to the steeper slope on the leeward side. Erosive processes are also clearly visible in present-day bathymetry (Figure 1b) and in the isopach map of S3 with the channel incision (more than 6 km wide) in the deep basin East of the seamount mentioned previously. A by-pass area is also visible between the main volcanic edifice of Grande Glorieuses and the rock islet located northward. Note that volumes estimated within S1, S2 and S3 correspond to respectively 27%, 37% and 36% of the entire sediment cover on slope and in the basin (3927 km^3).

5.3. VERTICAL PLATFORM MOVEMENTS

Figure 9c spatially replaces dredge datings along the flank of the platform and shows inferred vertical movements from these data. Before any interpretative work, it is important to keep in mind that rock sampling with dredge is associated with two main types of uncertainty. First, rock samples are frequently associated with a significant uncertainty as to their precise location with respect to distance, geometry and topography of the dredge path on the seafloor. While water depth represents a key parameter in the study of drowned shallow-water carbonate platforms, dredged carbonate samples are commonly associated with several hundreds of meters of water depth. In this study, it must be noted that uncertainties associated with depth (Table 1) range from a few meters for shallower samples (DW4809A) to 115 m for deeper samples (DW4815); these uncertainties are much bigger than sea-level variations from Paleogene to present-day (-57 m from Miller et al, 2005). Second, dredging operations carried out along steep slopes can also sample reworked fallen blocks and pebbles whose original location was shallower than estimated dredge path, which can lead to major misinterpretations.

However, despite these caveats, Table 1 clearly shows that: (i) the ages provided by the two methods are consistent for all samples; (ii) two samples collected in the same dredge provide the same results (see DW4819A & DW4819B in Table 1) ; (iii), two samples collected at the same geographic coordinates but at different depths are consistent (see DW4814 : ~700m/~7 Ma vs 4815 : ~950 m/~35 Ma in Figure 9) ; and (iv) two samples collected at same depths but on different flanks of the seamount (see DW4814 and DW4819 in Figure 9) lead also to the same approximate age (~Late Tortonian/Early Messinian). We are thus rather confident for considering ages of our samples as true with no reworking.

Given that an increasing depth for a younger sample indicates an uplift phase (if we assume no reworking), and a decreasing depth for a younger sample corresponds to either subsidence or platform

aggradation, we can infer the vertical movement indicated on Figure 9. From Paleogene (~62 Ma) until today, the Glorieuses platform underwent alternating subsidence and uplift phases: (i) an uplift (148-262 m) occurred within the time interval 62-35 Ma, resulting in Priabonian carbonate underlying Paleogene carbonate; (ii) a subsidence phase (23-28 $m.Myr^{-1}$) drowned and backstepped the platform, before (iii) a significant uplift (421-435 m) occurred again during the Tortonian; (iv) since the Late Messinian, a rather strong subsidence (~100 $m.Myr^{-1}$) is currently drowning the platform (subsidence rate is four times greater relative to the Oligocene/Miocene subsidence phase). Taking into account the results from dredges, we can thus conclude that the Glorieuses carbonate platform has not evolved in an overall stable geodynamical setting since Early Paleogene times. Given that no tectonic imprints are visible along the Glorieuses seamount, these changes may be linked to long-wave deformation related to tectonic events in the adjacent areas.

However, the Late Paleocene Terrace located at 750m of water depth along the NW flank of the Glorieuses carbonate platform, is not typified by any diagenetic or geomorphologic evidences of emersion and associated dissolution/erosion processes (Courgeon et al., 2016). The lack of karstic features on this terrace indicate that the interpretation of the first uplift phase (62-35Ma) has to be assessed with caution. A possible explanation for the absence of karstification features on the relatively shallow Paleocene terrace (compared to Late Eocene shallow-water samples; DW4815, Table 1) would be differential subsidence/uplift rates between this terrace and the main Glorieuses Seamount during Paleogene times.

The chronostratigraphic evolution of the Glorieuses seamount and surrounding basin is re-built in 3D (Figure 11), showing the successive geometries and paleo-bathymetries of the seamount at ~65 Ma (top of S1a), at ~35 Ma (top of S1b), at ~15 Ma (top of S2?), and at present-day (top of S3). Figure 11 takes into account the vertical movements estimated in this study. Depth (m) relative to present-day sea-level is reconstructed at each considered time-step, taking into account subsidence history (this study) and sea-level variations (Miller et al., 2008). The geometry of the possible shallow-water carbonate production on the platform, and the simultaneous sedimentation in the surrounding basin are illustrated. It thus illustrates the global backstepping of the carbonate factory in the study area over the Neogene, and the simultaneous sediment infilling (S1 to S3) in the deep surrounding basin.

6. DISCUSSION

The stratigraphic units identified in this study are placed in a chronostratigraphic framework and correlated to the main geological events that could have potentially impacted the stratigraphic record (Figure 12). The correlation of our observations to global and/or regional events (climatic and hydrodynamic changes, magmatic pulses, timing of uplifts) and to stratigraphic records in the

surrounding areas lead us to suggest and discuss a long-term evolution scenario for the Glorieuses stratigraphy, including triggering factors.

A TURONIAN EMERGENCE OF THE VOLCANIC SEAMOUNT

From seismic stratigraphy (4.1.2 section), the volcanic emergence of Glorieuses seems to have occurred during the Turonian, much earlier than Geyser-Zélée banks (at the Cretaceous-Paleogene transition), Mayotte island (at Late Paleogene to Neogene), and, *a fortiori* earlier than the other Western Comoro islands whose volcanism is dated to an even younger age (Nougier et al., 1986, Michon et al., 2019).

It's also interesting to note that the dated dredge samples with an age of 69 Ma constitute one of superficial formations of the volcanic edifice. Its evolved composition is coherent with the late stage evolution of the volcano as observed on other shield volcanoes (Peterson and Moore, 1987; Bachèlery, 1999). Therefore, petrological analyses also appear to support the hypothesis that the Glorieuses volcanic edifice is older than 69 Ma.

Turonian emergence of the Glorieuses Seamount corresponds to a well-known volcanic pulse related to the end of the Gondwana break-up and the rifting of India-Seychelles from Madagascar (Plummer et al., 1995; Storey et al., 1995; Cucciniello et al., 2013). This pulse is recorded (i) in the Diego Basin, North of Madagascar (Coffin, 1988), but also (ii) in the Majunga Basin with the exposed Majunga Flood Basalt (Coffin, 1988) that has been recently estimated to have started about 92 Ma (Cucciniello, 2013; Jafar, 2016). This age seemingly excludes a link with the volcanic activity recorded in the Comoros Archipelago and that has been recently interpreted as resulting from a lithospheric deformation in relation to the East African Rifting during late Cenozoic times (Michon, 2016, Bachèlery and Hémond, 2016). Conversely, the birth of Glorieuses is synchronous with a kinematic regional event that relates the initial inception of Glorieuses more closely with the seamounts capped by coralline outer Seychelles.

The structural fabric of the Glorieuses seamount shows 2 main directions: NNW-SSE and WSW-ENE (red straight lines in the bottom part of Figure 10a). These correspond to the directions of the fractures related to the successive openings of the Somali (Early Cretaceous) and Mascareigne (Late Cretaceous) basins (Bernard & Munschy, 2000). The edification of the Glorieuses seamount is thus likely controlled by successive regional kinematic events leading to rejuvenated volcanism that used inherited fractures (possibly until present-day). Thus, we suggest that the initial and main phase of the volcanic edification of the Glorieuses occurred at around the Cenomanian/Turonian transition, but with a possible poly-phased emergence, explaining later volcanic pulses seen on seismic data. A secondary volcanic pulse likely occurred during the Maastrichtian coeval to the break-up of Madagascar and Greater India during late Cretaceous times (Storey et al., 1995).

VOLCANIC PHASES

Seismic lines (Figures 2 to 7) suggest several volcanic features within the sediment infill above the volcanic basement. It includes: (1) probably volcano-clastic material (named V0 in Figure 12) within the Turonian unit S0; (2) large sills within the Sequence S1a (Figure 5), with a particular well-expressed one at the top of S1a that corresponds to the K/T boundary (we called it V1 in Figure 12); (3) stacking pattern of very high reflectivity within the almost entire S2a (Figure 6 & V2 in Figure 12); (4) a continuous very high amplitude reflection at the top of S2b which is better expressed on the windward side (Figure 6 & V3 in Figure 12). V0 and V1 features may be consistent with successive Turonian and Maastrichtian magmatic pulses, respectively dated with seismic chrono-stratigraphy and geochemistry. The question remains as to whether very strongly reflective reflectors within S2a (V2) and at the top of S2b (V3) may represent volcanic eruptions. It is tempting to relate V2 and V3 to volcanic accretion pulses that might explain the two apparent uplifts deduced from preserved records of carbonate terraces. Within the low-resolution time interval defined previously (62 Ma-35 Ma), Priabonian-Oligocene (Late Eocene) volcanism, known to also occur in the very close Diego Basin (North Madagascar) (Coffin and Rabinotwitz, 1988) appears to be a consistent candidate that may explain the apparent uplift of ~148-262 m. In the same speculative way, we suggest a possible causal relationship between volcanic pulse V3 and the 421-435 m Tortonian uplift phase previously evidenced.

Significant stages of exhumation in the South African Plateau have been documented in the Late Cretaceous ~65 Ma (King, 1967; Brown et al., 1990; Gallagher and Brown, 1999; Tinker et al., 2008a, b; Kounov et al., 2009) and since the Oligocene (30 Ma; Burke, 1996; Burke and Gunnell, 2008). These were initiated at ~23 Ma, most likely due to an uplift event of the North-eastern part of the South African Plateau (Said et al., 2015). Two main periods of uplift were documented during the thermal subsidence stage of the Agulhas Margin: (i) a 92-Ma short-lived margin-scale uplift, followed by a second one at 76 Ma located along the Outeniqua Basin, and; (ii) a long-lasting uplift from 40 to 15 Ma limited to the Durban (Thekwini) Basin (Baby et al., 2018). This suggests that the South African Plateau is an old Upper Cretaceous feature (90–70 Ma) reactivated during Late Eocene to Early Miocene times (40–15 Ma).

These uplift stages are synchronous with observed increase in sediment flux in the Mozambique Basin from the Zambezi River over two periods: (i) since Late Cretaceous (90-65 Ma) related to a rapid denudation of southern Africa after a tectonic uplift (Castelino et al., 2015); and (ii) during Late Oligocene- Early Miocene times (34 -23 Ma) caused by an uplift at a continental scale by 300-500 m. A third stage (iii) has been recognized since the Late Miocene (Walford et al., 2005) notably because of a Late Pliocene regional uplift of 900 m (Partridge and Maud, 1987).

In Madagascar, deformation is characterized by (i) a northward tilt during Late Cretaceous, followed by (ii) a rather quiet tectonic phase during Paleocene and Early Eocene (66 -34 Ma), before (iii)

a doming phase. The Late Miocene is the paroxysm of uplift with (i) a tilting of the margin (Morondova), (ii) an increase of the siliciclastic sand flux since middle Miocene, and (iii) a major stepping of planation surfaces. The end result of this uplift is a convex-up-shaped pattern for the Late Cretaceous surface and a large degree of weathering during Eocene times that creates the present-day dome morphology of Madagascar. The amplitude of this uplift can be estimated to around 850 m, with a very long wavelength deformation (x1000 km) that must be explained by mantle dynamics (Delaunay, 2018).

In this study, two apparent uplift phases (related to magmatic pulses) are recognized at Glorieuses isolated seamount: (i) during Early or middle Paleogene (between 62 Ma and 35 Ma) but likely during Late Eocene, and (ii) during Late Tortonian/Early Messinian (~ 9.5 Ma-7 Ma), with respective amplitudes of ~200 m and ~425 m. These two events are thus synchronous of uplift paroxysm at a larger scale (at Madagascar and/or South Africa scales).

BOTTOM CURRENTS: A STRONG AND REGIONAL IMPACT SINCE THE EOCENE

The basinal part of S1 clearly shows a distinct (transparent) facies from the overlying sequences (S2 and S3). It is characterized on the slope by the development of elongated contourite drifts initiated directly above the volcanic seamount leeward flanks. Thus, the top of S1 probably reflects a regional change affecting the nature of sedimentation both on leeward and windward sides of the island. Cessation of the contourite drifts and the erosion observed on their top within the upper part of S1 is likely related to bottom current changes at that time. Sedimentation rates in contourite drifts can be up to one order of magnitude higher than in pelagic sediments, making contourite drifts advantageous targets for high resolution palaeoceanographic and palaeoclimatic studies (Knutz, 2008; McCave, 2008). Possibly the most important point emanating from a large volume of work on erosional, isotopic and other signatures from Cenozoic drift deposits is that episodes of major increase in bottom circulation seem to correspond to periods of climatic instability. These lead to widespread erosional rather than depositional events within the contourite record (Faugères & Stow, 1993).

Important changes that affected continental margin sedimentation in the West Indian Ocean occurred in the Cenomanian/Turonian (90-100 million years ago), at the Cretaceous/Tertiary boundary (65 Myr ago), in the Oligocene (38 - 22 Myr ago) and at the Miocene/Pliocene boundary (5 Myr ago) (Flemming, 1980; Ramsay, 1994). Changes in the Agulhas Current regime may have contributed to the events in the Cenomanian/Turonian and at the end of the Cretaceous (Martin *et al.,* 1982). Indeed, close to the Cenomanian Turonian boundary (93 Ma) a change from an euxinic to an open marine sedimentation regime occurred in the Diego Basin as a result of the opening of several oceanic gateways including the Mozambique channel. Since their location directly overlies the Turonian volcanic basement, initiation of the elongated contourite drifts could thus have occurred during the Late Cretaceous (~ 93 Ma) within S1a or during the Early Paleogene (~65 Ma) within S1b.

As described by Ben-Avraham et al. (1994), the Eocene/Oligocene boundary in the Indian Ocean is marked by a widespread hiatus due to erosion, and an increase in current bedforms linked to the development of high-velocity bottom currents (the cold Antarctic Bottom Water).The Eocene/Oligocene boundary (~35 Ma) could thus be a relevant candidate to date the cessation of the elongated contourite drifts and erosional basinal surface corresponding to the top of S1b. It thus implies that these contourite drifts mainly developed during the Eocene.

This timing would also explain the facies change between sequences S1 and S2. Paleo-oceanographic modelling has demonstrated that throughout the Paleogene, the prevailing current was actually eastward towards Madagascar and the Seychelles, in contrast to the present-day configuration [Figure 12] (Ali & Huber, 2010; Townsend et al., 2010). This implies that, before ~38-35 Ma, major hemipelagic sedimentation in the basins surrounding Glorieuses would have originated from East Africa, and sediments would have been distributed by eastward flows. After that time, basins near the Glorieuses Archipelago would have been mainly fed by detrital input from the (North)western margin of Madagascar (and easternmost sources), distributed by a westward flow as it appears at the present-day. Note that this transition represents the chronostratigraphic equivalent of the "green" horizon from Coffin & Rabinotwitz (1988; 1992), and the "A0" horizon in the North Mozambique margin, on the East African Rift System (EARS) from Mougenot et al. (1986).

It is also noteworthy that the ages attributed by Schlüter & Uenzelmann-Neben (2007) within the Transkei Basin (offshore South Africa) for the tops of their 1A and 1B units (whose seismic facies were surprisingly similar to S1a and S1b units in this study- Figure 6) respectively correspond to the Cretaceous/Tertiary and Eocene/Oligocene boundaries. This is therefore in entire agreement with our suggested age model for the lowermost units.

Climate variations probably influence sedimentation since the Late Eocene. The top of S1b corresponds to a major oceanographic change at the Eocene/Oligocene boundary (~35 Ma) but it also corresponds to a global climate-warming episode (Figure 12). Warming at that time may thus explain why S2 is characterized by the initiation of two local contrasting sediment infillings between leeward and windward sides. MTCs appear within the upper part of sequence S2 (S2b unit) with two major events: one is limited to the leeward side, the other on the windward side (note also the larger size of this latter) [Figures 3,4,5]. Whilst the first probably originated from the destabilization of the west flank of the Glorieuses, the latter appears to originate from North Madagascar (Figure 10). The uppermost part of sequence S2 is therefore characterized by larger-scale destabilization processes.

These destabilizations are probably related to Madagascar and the northern adjacent basins uplift during the Mid-Miocene (Delaunay, 2018) [Figure 12]. The age of the top of unit S2a would thus be estimated to the Middle Miocene. In such a scenario, the synchronous onset of the modern South

Asian monsoon winds around 12.9 Ma (Betzler et al., 2016) could also have contributed to increased erosional (winnowing) and gravity processes (slope destabilization) at that time. Note that the (O) reflector, defined in both the Rovuma Basin and at DSDP Site 242 and dated at the top of the Oligocene (~23 Ma) (Franke et al., 2015), which is equivalent to the horizon A1 of Mougenot et al. (1986), could be picked within S2a.

The presence of canyons that are known to cut into the middle Miocene strata (Walford et al., 2005) give hints on identifying a late Miocene reflector (LM) in the Rovuma Basin on the offshore branch of the East African Rift System (Franke et al., 2015). Here, sequence S3 is characterized by large erosive processes: a prominent incised channel is particularly visible on the deep basin, East of the Glorieuses seamount. It is not inconsistent that the top of S2b unit (base of S3 sequence) corresponds to a Middle Miocene reflector, following the A2 reflector from Mougenot et al., (1986). The top of the S3a unit may thus be chronologically equivalent to the A3 reflector of Mougenot et al. (1986) in the EARS and to the LM reflector from Franke et al. (2015) in the Rovuma Basin and DSDP Site 242 (location in Figure 1, e.g. Simpson et al., 1974). As for S2b unit, during S3, the increase of Asian monsoon and/or climate variability during Pliocene and Pleistocene (Gupta, 1997) may have likely affected the production and transport of shallow-water sediment, leading to sediment export from the platform/upper slope towards the deep basin.

If we calculate sediment rate from previously estimated volumes (Figure 10b) according to the proposed age model (Figure 12), it results the rough following sediment rates within S1 (~90-35 Ma), S2 (~35-10 Ma), and S3 (~10-0 Ma): ~25 $km^3.Myr^{-1}$, ~58 $km^3.Myr^{-1}$, 105 $km^3.Myr^{-1}$. These values show the same trends than the DSDP 242with two successive increases by twice: (i) at the Eocene/Oligocene transition and (ii) at the End of Miocene. These values, even if they are rough estimates (time-depth conversion with constant velocity, no distinction between lithology and no porosity correction…), provide respective orders of magnitude of (i) the impact of both climate and oceanographic changes leading to a drastic reorganisation in sediment supplies, and (ii) the concomitant impact of both tectonic (uplift) and climatic deterioration (monsoon initiation and variability increase).

7. CONCLUSION

Previous studies combining geophysical and geological data have already pointed out morphological features that guide our understanding of the evolution of the Glorieuses platform. The flanks of the platform and nearby areas are characterized by flat-topped morphologies and associated slope breaks at around 1100 m, 750m and 200 m water depths. These terraces are located on a submarine ridge, the top of which occurs at −1000 m water depth, NW of the Glorieuses Platform. A coralgal limestone sampled on top of the 750 m deep terrace has been dated at 61.52 ± 1.80 Ma, which suggests that this drowned terrace developed in a shallow-water depositional environment during the Paleocene (at the latest). Overall, the distinct terrace levels observed are interpreted as resulting from

successive development and backstepping episodes, before the initiation of modern shallow-water carbonate systems (Courgeon *et al.,* 2016).

The main results can be summarized as follows: (i) the volcanic Glorieuses seamount probably emerged from a Late Cretaceous (Turonian) magmatic pulse; (ii) at least two significant uplift phases are recognized during the Tertiary (the Paleogene and/or the Eocene and the Tortonian); (iii) Glorieuses basinal sedimentation records an abrupt change probably related to major regional hydro-dynamical changes in Late Eocene times in the West Indian Ocean; (iv) the export of sediments from the platform towards the basin (numerous gravity flow processes) is strongly enhanced after the Mid-Late Miocene with probable increased production/shallow erosion led by the onset of the Asian monsoon winds and bipolar circulation.

Finally, Glorieuses seamount, although located in the vicinity of the Comoros, appears to have experienced a much longer history than these islands, and has a geological history closer to that of the Seychelles or the northern tip of Madagascar. Moreover, the SSE-NNW structural orientation of the alignment from the Leven bank (North Madagascar)-Glorieuses-Aldabra to Cosmoledo atoll (within the outer Seychelles-Figure 1) also suggests that volcanism re-uses fracture zones inherited from the Somali Basin opening. Further studies dedicated to dating and characterization of the volcanism within the overall area (not only Glorieuses seamount, but also the Comoro, Cosmoledo and Seychelles archipelagos) are currently in progress.

ACKNOWLEDGEMENTS

We are indebted to Captain, Officers, crew members and the scientific teams of PTOLEMEE, Biomaglo and PAMELA-MOZ01 cruises. The PTOLEMEE expedition is part of the PAMELA (Passive Margin Exploration Laboratory) scientific project funded by TOTAL. The Biomaglo cruise belongs to the Tropical Deep-Sea Benthos Program and was co-funded by the MNHN and the TAAF. We are also grateful to Massimo Dall 'Asta from TOTAL as well as ION for additional seismic data contributions. We also thank François Guillocheau & Cécile Robin for helpful discussions related to this project. We also want to thank the Guest Editor Wilfried Jokat and three anonymous reviewers who greatly improved the initial version of this paper. Alison Chalm is warmly thanked for the final English proofreading.

REFERENCES

Ali, J. R., & Huber, M. (2010). Mammalian biodiversity on Madagascar controlled by ocean currents. Nature, 463(7281), 653.

Andréfouët S, Chagnaud N, Chauvin C, & Kranenburg C.J. (2008). Atlas of French Overseas coral reefs. Centre IRD-Nouméa, Nouvelle-Calédonie.

Baby, G., Guillocheau, F., Boulogne, C., Robin, C., & Dall'Asta, M. (2018). Uplift history of a transform continental margin revealed by the stratigraphic record: The case of the Agulhas transform

margin along the Southern African Plateau. Tectonophysics, 731, 104-130. https://doi.org/10.1016/j.tecto.2018.03.014

Bachèlery, P. (1999). Le Fonctionnement des volcans boucliers. Mémoire HDR, Université de La Réunion.

Bachèlery, P., & Hémond, C. (2016). Geochemical and Petrological Aspects of Karthala Volcano. In Active Volcanoes of the Southwest Indian Ocean (pp. 367-384). Springer, Berlin, Heidelberg.

Battistini, R., & Cremers, G. (1972). Geomorphology and vegetation of Iles Glorieuses. Atoll Research Bulletin.

Battistini, R., Gayet, J., Jouannic, C., Labracherie, M., Peypouquet, J. P., Pujol, C., ... & Turon, J. L. (1976). Etude des sédiments et la microfaune des îles Glorieuses (Canal de Mozambique). Cahiers ORSTOM. Série Géologie, 8(2), 147-171.

Battistini, R., Lalou, C., & Elbez, G. (1976). Datation par la méthode 230Th 234U du Pléistocene moyen marin de Madagascar et des ıles voisines. CR somm Soc géol France, 5, 201.

Bardintzeff, J. M., Liégeois, J. P., Bonin, B., Bellon, H., & Rasamimanana, G. (2010). Madagascar volcanic provinces linked to the Gondwana break-up: Geochemical and isotopic evidences for contrasting mantle sources. Gondwana Research, 18(2-3), 295-314. doi:10.1016/j.gr.2009.11.010

Ben-Avraham, Z., Niemi, T. M., & Hartnady, C. J. (1994). Mid-Tertiary changes in deep ocean circulation patterns in the Natal Valley and Transkei Basin, Southwest Indian Ocean. Earth and Planetary Science Letters, 121(3-4), 639-646. https://doi.org/10.1016/0012-821X(94)90097-3

Bernard, A., & Munschy, M. (2000). Were the Mascarene and Laxmi Basins (western Indian Ocean) formed at the same spreading centre? Comptes Rendus De L Academie Des Sciences Serie Ii Fascicule a-Sciences De La Terre Et Des Planetes, 330(11), 777-783. https://doi.org/10.1016/S1251-8050(00)00221-4

Betzler, C., Eberli, G. P., Kroon, D., Wright, J. D., Swart, P. K., Nath, B. N., ... & Guo, J. A. (2016). The abrupt onset of the modern South Asian Monsoon winds. Scientific reports, 6, 29838. https://doi.org/10.1038/srep29838

BouDagher-Fadel, M. K. (2008). Evolution and geological significance of larger benthic foraminifera. Developments in Palaeontology and Stratigraphy 21, 1–548.

BouDagher-Fadel, M. K. (2015). Biostratigraphic and Geological Significance of Planktonic Foraminifera. UCL Press, London (298pp.).

BouDagher-Fadel M. K. (2018a). Evolution and geological significance of larger BenthicForaminifera. London: UCL Press (704 p.)

BouDagher-Fadel M. K. (2018b). Revised diagnostic first and last occurrences of Mesozoic and Cenozoic planktonic foraminifera. UCL Office of the Vice-Provost Research, Professional Papers Series, UCL Press, p. 1–5.

Brereton, N. R. (1970). Corrections for interfering isotopes in the 40 Ar/39 Ar dating method. Earth and Planetary Science Letters. Elsevier **8**, 427–433.

Brown, R. W., Rust, D. J., Summerfield, M. A., Gleadow, A. J., & De Wit, M. C. (1990). An Early Cretaceous phase of accelerated erosion on the south-western margin of Africa: Evidence from apatite fission track analysis and the offshore sedimentary record. International Journal of Radiation Applications and Instrumentation. Part D. Nuclear Tracks and Radiation Measurements, 17(3), 339-350. https://doi.org/10.1016/1359-0189(90)90056-4

Burke, K. (1996). The African plate. South African Journal of Geology, 99(4), 341-409.

Burke, K., & Gunnell, Y. (2008). The African erosion surface: a continental-scale synthesis of geomorphology, tectonics, and environmental change over the past 180 million years (Vol. 201). Geological Society of America.

Castelino, J. A., Reichert, C., Klingelhoefer, F., Aslanian, D., & Jokat, W. (2015). Mesozoic and Early Cenozoic sediment influx and morphology of the Mozambique Basin. Marine and Petroleum Geology, 66, 890-905. doi: 10.1016/j.marpetgeo.2015.07.028

Class, C., Goldstein, S.L., Altherr, R. & Bachèlery, P. (1998). The process of plume–lithosphere interactions in the ocean basins—the case of Grande Comore. J Petrol 39 (5) : 881–903. doi: 10.1093/petroj/39.5.881

Coffin, M.F. & Rabinowitz, P.D. (1987). Reconstruction of Madagascar and Africa: evidence from the Davie fracture zone and western Somali basin. J Geophys Res 92(B9):9385–9406. https://doi.org/10.1029/JB092iB09p09385

Coffin, M. F., & Rabinowitz, P. D. (Eds.). (1988). Evolution of the conjugate East African-Madagascan margins and the western Somali Basin (Vol. 226). Geological Society of America.

Coffin, M. F. & Rabinowitz, P. D. (1992). The Mesozoic East African and Madagascan conjugate continental margins: stratigraphy and tectonics: chapter 12: African and Mediterranean Margins.

Cohen, K.M., Finney, S.C., Gibbard, P.L. and Fan, J.-X., 2013, updated 2017. The ICS International Chronostratigraphic Chart. Episode **36**, 199-204. http://www.stratigraphy.org/index.php/icschart-timescale

Corbari L., Samadi, S. & Olu, K. (2017). BIOMAGLO cruise, RV Antéa. https://doi.org/10.17600/17004000.

Courtillot, V., Davaille, A., Besse, J., & Stock, J. (2003). Three distinct types of hotspots in the Earth's mantle. Earth Planet. Sci. Lett. 205: 295–308. doi: 10.1016/S0012-821X(02)01048-8

Cochran, J. R. (1988). Somali Basin, Chain Ridge, and origin of the Northern Somali Basin gravity and geoid low. Journal of Geophysical Research: Solid Earth, 93(B10), 11985-12008.

Counts, J. W., Jorry, S. J., Leroux, E., Miramontes, E., & Jouet, G. (2018). Sedimentation adjacent to atolls and volcano-cored carbonate platforms in the Mozambique channel (SW Indian Ocean). Marine Geology, 404, 41-59. https://doi.org/10.1016/j.margeo.2018.07.003

Courgeon, S., Jorry, S. J., Camoin, G. F., BouDagher-Fadel, M. K., Jouet, G., Révillon, S., ... & Droxler, A. W. (2016). Growth and demise of Cenozoic isolated carbonate platforms: New insights from the Mozambique channel seamounts (SW Indian Ocean). Marine Geology, 380, 90-105.

Courgeon, S., Jorry, S. J., Jouet, G., Camoin, G., BouDagher-Fadel, M. K., Bachèlery, P., ... & Thereau, E. (2017). Impact of tectonic and volcanism on the Neogene evolution of isolated carbonate platforms (SW Indian Ocean). Sedimentary Geology, 355, 114-131. https://doi.org/10.1016/j.sedgeo.2017.04.008

Cox, K. G. (1992). Karoo igneous activity, and the early stages of the break-up of Gondwanaland. Geological Society, London, Special Publications, 68(1), 137-148.

Cucciniello, C., Melluso, L., Jourdan, F., Mahoney, J. J., Meisel, T., & Morra, V. (2013). 40 Ar–39 Ar ages and isotope geochemistry of Cretaceous basalts in northern Madagascar: refining eruption ages, extent of crustal contamination and parental magmas in a flood basalt province. Geological Magazine, 150(1), 1-17. doi:10.1017/S0016756812000088

Dalrymple, G. B. & Lanphere, M. A. (1971). 40 Ar/39 Ar technique of K Ar dating: a comparison with the conventional technique. *Earth and Planetary Science Letters*. Elsevier **12**, 300–308.

Darwin, C. (1842). The structure and distribution of coral reefs, 2nd ed. Smith Elder and Co, London, 95 p.

Delaunay, A. (2018). Les mouvements verticaux de Madagascar (90 - 0 Ma) : une analyse couplée des formes du relief et de l'enregistrement sédimentaire des marges ouest malgaches. PhD report, Univ. Rennes 1., 367 p.

Eagles, G. & König, M. (2008). A model of plate kinematics in Gondwana breakup. Geophys. Journ. Internat., 173, 703– 717. doi: 10.1111/j.1365-246X. 2008.03753.x.

Emerick, C.M. & Duncan, R.A. (1982). Age progressive volcanism in the Comores Archipelago, western Indian Ocean and implications for Somali plate tectonics. Earth Planet. Sci. Lett. 60(3): 415–428.

Faugères, J. C., & Stow, D. A. (1993). Bottom-current-controlled sedimentation: a synthesis of the contourite problem. Sedimentary Geology, 82(1-4), 287-297.

Flemming, B.W. (1980) Sand transport and bedform patterns on the continental shelf between Durban and Port Elizabeth (southeast African continental margin). Sed. Geol., 26, 179–205.

Flores, G. (1984). The SE Africa triple junction and the drift of Madagascar. Journal of Petroleum Geology, 7(4), 403-418.

Förster, R. 1975. The geological history of the sedimentary basin of southern Mozambique, and some aspects of the origin of the Mozambique channel. Palaeogeography, Palaeoclimatology, Palaeoecology, 17, 267-287.

Franke, D., Jokat, W., Ladage, S., Stollhofen, H., Klimke, J., Lutz, R., ... & Schreckenberger, B. (2015). The offshore East African Rift System: Structural framework at the toe of a juvenile rift. Tectonics, 34(10), 2086-2104. https://doi.org/10.1002/2015TC003922

Gallagher, K., & Brown, R. (1999). Denudation and uplift at passive margins: the record on the Atlantic Margin of southern Africa. Philosophical Transactions of the Royal Society of London. Series A: Mathematical, Physical and Engineering Sciences, 357(1753), 835-859. https://doi.org/10.1098/rsta.1999.0354

Gaven, C., & Vernier, E. (1979). Datation Io. U de coraux et paléogéodynamique du Pléistocène moyen des Iles Glorieuses (Canal du Mozambique). Quaternaria. Storia Naturale e Culturale del Quaternario Roma, 21, 45-52.

Grenard-Grand, E. (2018). Géomorphologie et évolution stratigraphique de la marge nord-ouest de Madagascar depuis le Crétacé : rôle des courants et des transferts sédimentaires dans l'incision de la pente continentale. Master 2 report, Univ. Perpignan, 53p.

Guillaume, M.M.M., Reyss, J.-L., Pirazzoli, P.A., & Bruggemann, J.H. (2013). Tectonic stability since the last interglacial offsets the Glorieuses Islands from the nearby Comoros archipelago. Coral Reefs 32, 719–726.

Gupta, A. K. (1997). Paleoceanographic and paleoclimatic history of the Somali Basin during the Pliocene-Pleistocene; multivariate analyses of benthic foraminifera from DSDP Site 241 (Leg 25). The Journal of Foraminiferal Research, 27(3), 196-208. https://doi.org/10.2113/gsjfr.27.3.196

Hanes, J.A., York, D., Hall, & C.M. (1985). An 40Ar/39Ar geochronological and electron microprobe investigation of an Archean pyroxenite and its bearing on ancient atmospheric compositions. Canadian Journal of Earth Science 22, 947-958. https://doi.org/10.1139/e85-100

Jafar, S. A. (2016). Episodes of subaerial Large Igneous Provinces (LIPs) linked to late Turonian/late Maastrichtian deep incursion of sea on the Indian continental block. Global Geology, 19(4), 255-260. doi:10. 3969 / j. issn. 1673-9736. 2016. 04. 06

Jokat, W., Boebel, T., König, M., & Meyer, U. (2003). Timing and geometry of early Gondwana breakup. Journal of Geophysical Research: Solid Earth, 108(B9). https://doi.org/10.1029/2002JB001802

Jorry, S.J., 2014. PTOLEMEE Cruise. RV L'Atalante. http://dx.doi.org/10.17600/14000900.

Jorry, S. J., Camoin, G. F., Jouet, G., Le Roy, P., Vella, C., Courgeon, S., ... & Caline, B. (2016). Modern sediments and Pleistocene reefs from isolated carbonate platforms (Iles Eparses, SW Indian Ocean): a preliminary study. Acta oecologica, 72, 129-143. https://doi.org/10.1016/j.actao.2015.10.014

Jourdan, F. & Renne, P. R. (2007). Age calibration of the Fish Canyon sanidine 40 Ar/39 Ar dating standard using primary K–Ar standards. *Geochimica et Cosmochimica Acta*. Elsevier **71**, 387–402. https://doi.org/10.1016/j.gca.2006.09.002

Kamen-Kaye, M. (1982). Mozambique-Madagascar geosyncline, I: deposition and architecture. Journal of Petroleum Geology, 5(1), 3-30. https://doi.org/10.1111/j.1747-5457.1982.tb00558.x

Kent, D. V., & Gradstein, F. M. (1985). A Cretaceous and Jurassic geochronology. Geological Society of America Bulletin, 96(11), 1419-1427. https://doi.org/10.1130/0016-7606(1985)96%3C1419:ACAJG%3E2.0.CO;2

Key, R. M., Smith, R. A., Smelror, M., Sæther, O. M., Thorsnes, T., Powell, J. H., ... & Zandamela, E. B. (2008). Revised lithostratigraphy of the Mesozoic-Cenozoic succession of the onshore Rovuma Basin, northern coastal Mozambique. South African Journal of Geology, 111(1), 89-108. https://doi.org/10.2113/gssajg.111.1.89

King, L.C. (1967). The Morphology of the Earth, Hafner, New York, 1967.

Klimke, J., & Franke, D. (2016). Gondwana breakup: no evidence for a Davie Fracture Zone offshore northern Mozambique, Tanzania and Kenya. Terra Nova, 28(4), 233-244. https://doi.org/10.1111/ter.12214

Knutz, P. C. (2008). Palaeoceanographic significance of contourite drifts. Developments in Sedimentology, 60, 511-535. https://doi.org/10.1016/S0070-4571(08)10024-3

König, M., & Jokat, W. (2010). Advanced insights into magmatism and volcanism of the Mozambique Ridge and Mozambique Basin in the view of new potential field data. Geophysical Journal International, 180(1), 158-180. https://doi.org/10.1111/j.1365-246X.2009.04433.x

Kounov, A., Viola, G., De Wit, M., & Andreoli, M. A. G. (2009). Denudation along the Atlantic passive margin: new insights from apatite fission-track analysis on the western coast of South Africa. Geological Society, London, Special Publications, 324(1), 287-306. https://doi.org/10.1144/SP324.19

Krause, D. W., Sertich, J. J., O'Connor, P. M., Rogers, K. C., & Rogers, R. R. (2019). The Mesozoic Biogeographic History of Gondwanan Terrestrial Vertebrates: Insights from Madagascar's Fossil Record. Annual Review of Earth and Planetary Sciences, 47. https://doi.org/10.1146/annurev-earth-053018-060051

Lee, J.-Y., Marti, K., Severinghaus, J.P., Kawamura, K., Yoo, H.-S., Lee, J.B., & Kim, J.S. (2006). A redetermination of the isotopic abundances of atmospheric Ar. Geochimica et Cosmochimica Acta 70, 4507–4512. https://doi.org/10.1016/j.gca.2006.06.1563Leinweber, V. T., & Jokat, W. (2011). Is there continental crust underneath the northern Natal Valley and the Mozambique Coastal Plains? Geophysical Research Letters, 38(14). https://doi.org/10.1029/2011GL047659

Lort, J. M., Limond, W. Q., Segoufin, J., Patriat, P., Delteil, J. R., & Damotte, B. (1979). New seismic data in the Mozambique channel. Marine Geophysical Researches, 4(1), 71-89.

Mahanjane, E. S. (2012). A geotectonic history of the northern Mozambique Basin including the Beira High – A contribution for the understanding of its development. Marine and Petroleum Geology 36, 1-12. doi:10.1016/j. marpetgeo.2012.05.007.

Mahanjane, E. S., Franke, D., Lutz, R., Winsemann, J., Ehrhardt, A., Berglar, K., & Reichert, C. (2014). Maturity and petroleum systems modelling in the offshore Zambezi Delta depression and

Angoche Basin, northern Mozambique. Journal of Petroleum Geology, 37(4), 329-348. https://doi.org/10.1111/jpg.12589

Martin, A. K., Goodlad, S. W., Hartnady, C. J. H., & Plessis, A. D. (1982). Cretaceous palaeopositions of the Falkland Plateau relative to southern Africa using Mesozoic seafloor spreading anomalies. Geophysical Journal International, 71(3), 567-579. https://doi.org/10.1111/j.1365-246X.1982.tb02784.x

Maugé, L. A., Ségoufin, J., Vernier, E., & Froget, C. (1982). Geomorphologie et origine des bancs du nord-est du canal de Mozambique—Ocean Indien occidental (geomorphology and origin of the reef-banks of the north-eastern Mozambique Channel—Western Indian Ocean). Marine Geology, 47(1-2), 37-55. https://doi.org/10.1016/0025-3227(82)90018-4

McArthur, J.M., Howarth, R. J. et al. (2012). Chapter 7 - strontium isotope stratigraphy. The Geologic Time Scale 2012, Boston, Elsevier, 127–144.

McCall, R. A. (1997). Implications of recent geological investigations of the Mozambique channel for the mammalian colonization of Madagascar. Proceedings of the Royal Society of London. Series B: Biological Sciences, 264(1382), 663-665. https://doi.org/10.1098/rspb.1997.0094

McCave, I. N. (2008). Size sorting during transport and deposition of fine sediments: sortable silt and flow speed. Developments in Sedimentology, 60, 121-142. https://doi.org/10.1016/S0070-4571(08)10008-5

Mcdougall, I. & Harrison, T. (1999). *Geochronology and thermochronology by the 40Ar/39Ar method.* New York: Oxford University Press.

Meert, J. G. & Tamrat, E. (2006). Paleomagnetic evidence for a stationary Marion hotspot: additional paleomagnetic data from Madagascar. Gondwana Research, 10(3-4), 340-348. https://doi.org/10.1016/j.gr.2006.04.008

Michon, L. (2016). The volcanism of the Comoros archipelago integrated at a regional scale. Bachelery, Patrick and Lénat, Jean-François and Di Muro, Andrea and Michon, Laurent. Active Volcanoes of the Southwest Indian Ocean: Piton de la Fournaise and Karthala, Springer-Verlag, pp. 233-244, Active volcanoes of the World, 978-3-642-31394-3. hal-01147339.

Miller, K. G., Kominz, M. A., Browning, J. V., Wright, J. D., Mountain, G. S., Katz, M. E., ... & Pekar, S. F. (2005). The Phanerozoic record of global sea-level change. science, 310(5752), 1293-1298. doi: 10.1126/science.1116412

Mitchum Jr, R. M., Vail, P. R., & Thompson III, S. (1977). Seismic stratigraphy and global changes of sea level: Part 2. The depositional sequence as a basic unit for stratigraphic analysis: Section 2. Application of seismic reflection configuration to stratigraphic interpretation.

Mougenot, D., Virlogeux, P., Vanney, J. R., & Malod, J. (1986). La marge continentale au Nord du Mozambique; résultats préliminaires de la campagne Md40/Macamo. Bulletin de la Societe Geologique de France, 2(3), 419-422. https://doi.org/10.2113/gssgfbull.II.3.419

Müller, R. D., Sdrolias, M., Gaina, C., & Roest, W. R. (2008). Age, spreading rates, and spreading asymmetry of the world's ocean crust. Geochemistry, Geophysics, Geosystems, 9(4). https://doi.org/10.1029/2007GC001743

Müller, C.O., & Jokat, W. (2019). The initial Gondwana break-up: A synthesis based on new potential field data of the Africa-Antarctica Corridor, Tectonophysics, 750, 301-328. doi: 10.1016/j.tecto.2018.11.008

Nicholas, C.J., Pearson, P.N., McMillan, I.K., Ditchfield, P.W., & Singano, J.M. (2007). Structural evolution of southern coastal Tanzania since the Jurassic. Journal of African Earth Sciences, 48, 273-297. https://doi.org/10.1016/j.jafrearsci.2007.04.003

Nougier, J., Cantagrel, J.M. & Karche, J .P. (1986). The Comores Archipelago in the western Indian Ocean: volcanology geochronology and geodynamic setting. J African Earth Sci. 5: 135–145. https://doi.org/10.1016/0899-5362(86)90003-5

Olu, K., 2014. PAMELA-MOZ1 Cruise. RV L'Atalante. http://dx.doi.org/10.17600/14001000.

Partridge, T. C., & Maud, R. R. (1987). Geomorphic evolution of southern Africa since the Mesozoic. South African Journal of Geology, 90(2), 179-208.

Phethean, J. J., Kalnins, L. M., van Hunen, J., Biffi, P. G., Davies, R. J., & McCaffrey, K. J. (2016). Madagascar's escape from A frica: A high-resolution plate reconstruction for the W estern S omali B asin and implications for supercontinent dispersal. Geochemistry, Geophysics, Geosystems, 17(12), 5036-5055. https://doi.org/10.1002/2016GC006624

Pelleter, A. A., Caroff, M., Cordier, C., Bachèlery, P., Nehlig, P., Debeuf, D., & Arnaud, N. (2014). Melilite-bearing lavas in Mayotte (France): An insight into the mantle source below the Comores. Lithos, 208, 281-297. https://doi.org/10.1016/j.lithos.2014.09.012

Peterson, D. W. & Moore, R. B. (1987). Geologic history and evolution of geologic concepts, island of Hawaii. *Volcanism in Hawaii*, **1350**, 149–189.

Plummer, P. S. (1995). Ages and geological significance of the igneous rocks from Seychelles. Journal of African Earth Sciences, 20(2), 91-101. https://doi.org/10.1016/0899-5362(95)00035-R

Prat, S., Jorry, S. J., Jouet, G., Camoin, G., Vella, C., Le Roy, P., ... & Pastol, Y. (2016). Geomorphology and sedimentology of a modern isolated carbonate platform: The Glorieuses archipelago, SW Indian Ocean. Marine Geology, 380, 272-283. https://doi.org/10.1016/j.margeo.2016.04.009

Rabinowitz, P.D., Coffin, M.F., & Falvey, D. (1983). The separation of Madagascar and Africa. Science 220 (4592): 67–69. doi: 10.1126/science.220.4592.67

Ramsay, P. J. (1994). Marine geology of the Sodwana Bay shelf, southeast Africa. Marine Geology 120, 225–247. https://doi.org/10.1016/0025-3227(94)90060-4

Rasamimanana, G., Bardintzeff, J.M., Rasendrasoa, J., Bellon, H., Thouin, C., Gioan, P., & Piqué, A. (1998). Les épisodes magmatiques du Sud-Ouest de Madagascar (bassin de Morondava), marqueurs des

phénomènes de rifting crétacé et néogène. C. R. Acad Sci 326 (10): 685–691. https://doi.org/10.1016/S1251-8050(98)80179-1

Reeves, C. (2000). The Geophysical mapping of Mesozoic dyke swarms in southern Africa and their origin in the disruption of Gondwana. Journal of African Earth Sciences 30, 449-513. https://doi.org/10.1016/S0899-5362(00)00035-X

Reeves, C. (2014). The position of Madagascar within Gondwana and its movements during Gondwana dispersal. Journal of African Earth Sciences, 94, 45-57. https://doi.org/10.1016/j.jafrearsci.2013.07.011

Roddick, J.C., Cliff, R.A., & Rex D.C. (1980). The evolution of excess argon in alpine biotites - A 40Ar-39Ar analysis. Earth and Planetary Science Letters 48, 185-208. https://doi.org/10.1016/0012-821X(80)90181-8

Said, A., Moder, C., Clark, S., & Abdelmalak, M. M. (2015). Sedimentary budgets of the Tanzania coastal basin and implications for uplift history of the East African rift system. Journal of African Earth Sciences, 111, 288-295. https://doi.org/10.1016/j.jafrearsci.2015.08.012

Salman, G. & Abdula, I. (1995). Development of the Mozambique and Ruvuma sedimentary basins, offshore Mozambique. Sedimentary Geology 96, 7-41. Elsevier Science B.V. SSDI 0037-0738(94)00125-1. https://doi.org/10.1016/0037-0738(95)00125-R

Schlüter, P., & Uenzelmann-Neben, G. (2007). Seismostratigraphic analysis of the Transkei Basin: A history of deep sea current controlled sedimentation. Marine Geology, 240(1-4), 99-111. https://doi.org/10.1016/j.margeo.2007.02.015

Simpson, E.S.W., Schlich, R. et al., (1974). In: E.S.W. Simpson, R. Schlich et al., Init. Rep. Deep Sea Drilling Project, Leg 25: 287-346, US Government Printing Office, Washington.

Storey, M., Mahoney, J. J., Saunders, A. D., Duncan, R. A., Kelley, S. P., & Coffin, M. F. (1995). Timing of hot spot—related volcanism and the breakup of Madagascar and India. Science, 267(5199), 852-855. doi: 10.1126/science.267.5199.852

Tetley, N., McDougall, I. & Heydegger, H. R. (1980). Thermal neutron interferences in the 40Ar/39Ar dating technique. *Journal of Geophysical Research: Solid Earth (1978–2012)*. Wiley Online Library **85**, 7201–7205. https://doi.org/10.1029/JB085iB12p07201

Thompson, J. O., Moulin, M., Aslanian, D., De Clarens, P., & Guillocheau, F. (2019). New starting point for the Indian Ocean: Second phase of breakup for Gondwana. Earth-science reviews. https://doi.org/10.1016/j.earscirev.2019.01.018

Tinker, J., de Wit, M., & Brown, R. (2008). Linking source and sink: Evaluating the balance between onshore erosion and offshore sediment accumulation since Gondwana break-up, South Africa. Tectonophysics, 455(1-4), 94-103. https://doi.org/10.1016/j.tecto.2007.11.040

Tinker, J., de Wit, M., & Brown, R. (2008). Mesozoic exhumation of the southern Cape, South Africa, quantified using apatite fission track thermochronology. Tectonophysics, 455(1-4), 77-93. https://doi.org/10.1016/j.tecto.2007.10.009

Toomey, M., Ashton, A.D., & Perron, J.T. (2013). Profiles of ocean islands coral reefs controlled by sea-level history and carbonate accumulation rates. Geology 41, 731–734. https://doi.org/10.1130/G34109.1

Townsend, T. M., Tolley, K. A., Glaw, F., Böhme, W., & Vences, M. (2010). Eastward from Africa: palaeocurrent-mediated chameleon dispersal to the Seychelles islands. Biology Letters, 7(2), 225-228.

Turner, G., Cadogan P. H. (1974). Possible effects of 39Ar recoil in 40Ar-39Ar dating. Proceedings of the Fifth Lunar Science Conference 2, 1601 -1615.

Walford, H. L., White, N. J., & Sydow, J. C. (2005). Solid sediment load history of the Zambezi Delta. Earth and Planetary Science Letters, 238(1-2), 49-63. https://doi.org/10.1016/j.epsl.2005.07.014

York D. (1969). Least squares fitting of a straight line with correlated errors. Earth Planet. Sci. Lett. 5, 320-324.

York D., Evensen N., Lopez-Martinez M., & De Basabe Delgado, J. (2005). Unified equations for the slope, intercept, and standard errors of the best straight line. Am. J. Phys 72(3), 367-375. https://doi.org/10.1119/1.1632486

Zachos, J., Pagani, M., Sloan, L., Thomas, E., & Billups, K. (2001). Trends, rhythms, and aberrations in global climate 65 Ma to present. science, 292(5517), 686-693. doi: 10.1126/science.1059412

FIGURE CAPTIONS

Figure 01: A) Location and bathymetry (Gebco, 2008) of the study area (black square) in the Southwest Indian Ocean, about 160 km northwest of Madagascar . The Glorieuses island is surrounded by several archipelagos: the Cosmoledo Atoll in the North, the Farquhar and Providence atolls, along with the Seychelles in the North-East, and the Comores archipelago in the West (Mayotte, Anjouan, Moheli and Grande Comores from East to West). The black triangle and the white square represent the respective locations of the Chesterfield borehole and the DSDP 242. B) Focus on the location of the seismic and dredge data (respective dotted black lines and stars) superimposed on the bathymetric mapof the study area. Bathymetric map here results from Ptolémée 2014 survey. Yellow stars correspond to dredges used for vertical movement estimates, the green star corresponds to the dredge used for dating and characterizing Glorieuses volcanism. Thick black lines correspond to seismic lines shown in this paper.

Figure 02: Key stages in the separation of Madagascar from its neighbours in Gondwana. (A) The initial 'fit' position at ~168 Ma. (B) 145 Ma (Berriasian). East Gondwana ceases to be a single plate at about this time as Antarctica starts to rotate clockwise. (C) 120 Ma (early Aptian). Somali Ocean between

Madagascar and Somalia fails, ocean between Antarctica–Australia and Greater India fully active. (D) 88 Ma (Coniacian). Immediately before the outbreak of the Marion mantle plume and the start of India's rapid NE-ward movement. (E) 66 Ma (start Paleocene). Deccan Traps being erupted; major plate reorganisation between India and Madagascar; Mascarene Basin headed for extinction. (F) Present situation with Comores volcanicity. Modified from Reeves, 2014.

Figure 03: Uninterpreted (on top) and interpreted (on bottom) seismic strike profile (PTO 306) located in the deep basin on the leeward side. See location on the bottom right corner and on Figure 01. Seismic facies correspond to three regional mega-sequences: S1 (green), S2 (red), S3 (yellow) above the acoustic basement (grey). Locally, a S0 unit (dark green) is identified within the basement lows. See the text for more explanation. Sub-units (a, b) are also identified within S1 and S2. See the text for more explanation.

Figure 04a: Uninterpreted (on top) and interpreted (on bottom) seismic dip profile (PTO 315) located on the leeward side. See location on Figures 01 and 02. Seismic facies show three regional mega-sequences: S1 (green), S2 (red), S3 (yellow) above the acoustic basement (grey). Locally, a S0 unit (dark green) is identified within the basement lows. Sub-units (a, b) are also identified within S2 and S3. See the text for more explanation.

Figure 05: Uninterpreted (on top) and interpreted (on bottom) seismic profile (PTO 337) located in the basinal part on the windward side. Location on Figure 01. Seismic facies show three regional mega-sequences: S1 (green), S2 (red), S3 (yellow) above the acoustic basement (grey). Sub-units (a, b) are also identified within S2 and S3. Geological features are highlighted within black squares: A (volcanism), B (transparent seismic facies overlaying older sills and suggested to be linked to fluid raisings), C (bright spots corresponding to 3 successive volcanic sills), D (Mass Transport Deposit), E (deformation linked to volcanic intrusion or faults?). See the text for more explanation.

Figure 06: A) Comparison of the stratigraphic record between the leeward and windward sides of Glorieuses Islands showing the same mega-sequences (S1, S2, S3) stacked in the basin over the volcanic basement. The stratigraphic markers bounding these mega-sequences are reported (Top S1, Top S2). Location of the focus on the leeward side is indicated in Figure 3 (PTO 306); location of the focus on the windward side is shown by a red rectangle in Figure 5 (PTO 337) B) Seismic profile (vertical scale in sec. twtt) modified from Schlüter & Uenzelmann-Neben, 2007 in the Transkei Basin (South of the Mozambique channel) displaying stacked patterns of seismic facies surprisingly similar to sequences

S1-S3 identified in this study. These sequences are indicated. C) Focus on the seismic profile B) in the Transkei Basin, shown at the same vertical scale as Ptolemee seismic lines in A).

Figure 07a: Uninterpreted (on top) and interpreted (on bottom) seismic mosaic (globally oriented NNE-SSW) imaging the Somalian Basin from the southern part of the Glorieuses seamount to the Majunga margin. This mosaic corresponds to the juxtaposition of several seismic sections and crosses over the Geyser-Zélée banks. The location of the crossing line GXT 1300 (see the following Figure 7b) is identified by a vertical thin dark line. See locations on Figure 1. Limits of the sequences previously identified (S1, S2, S3 respectively in green, red, and yellow) have been elongated, allowing relative chrono-stratigraphy within the area to be viewed. It is noteworthy that the main volcanic phase of Geyser-Zélée is identified within Age Unit S2 (chrono-stratigraphic equivalent of S2 sequence), well after the edification of Glorieuses seamount.

Figure 07b: Interpreted compiled seismic sections (NNW-SSE) GXT 1300 showing the stratigraphic relationship between Mayotte and the Majunga margin. Location in Figure 1. This section crosses over the PTO-276c seismic profile illustrated on Figure 7a. Limits of the sequences previously identified (S1, S2, S3 respectively in green, red, and yellow) have been extended, allowing relative chrono-stratigraphy within the area to be viewed. It is noteworthy that the main volcanic phase of Mayotte island is identified within Age Unit S2 (chrono-stratigraphic equivalent of S2 sequence), long after the edification of Glorieuses seamount. With the courtesy of ION and Total.

Figure 07c: Interpreted compiled seismic sections showing the stratigraphic relationship between Mayotte, Geyser-Zélée banks, and the Glorieuses seamount. Location in Figure 1. Limits of the sequences previously identified (S1, S2, S3 respectively in green, red, and yellow) have been extended, allowing relative chrono-stratigraphy within the area. This single figure clearly synthesizes the previous ones (6a & 6b) to illustrate that the main volcanic phase of Mayotte, identified within Age Unit S2 (chrono-stratigraphic equivalent of S2 sequence), began well after the edification of Glorieuses seamount (Turonian), and also slightly after Geyser-Zélée banks (Top S2, ~35 Ma). With the courtesy of ION and Total.

Figure 08: A) Transmitted-light photomicrographs of microlitic DR04-10 sample with plagioclases and oxides microlites. Pl: plagioclase, px: clinopyroxene, ox: Fe-Ti oxides.**B)** Transmitted-light photomicrographs of porphyric microlitic DR04-11 sample with plagioclase and pyroxene phenocrysts in a groundmass made of sanidine laths and oxides. Pl: plagioclase, px: clinopyroxene, ox: Fe-Ti oxides. **C)** ^{39}Ar–^{40}Ar age spectra and $^{37}Ar_{Ca}/^{39}Ar_{K}$ spectra of samples DR04-10 and DR04-11. Apparent age error bars are at the 1σ level; errors in the J-parameter are not included. Plateau age is given with 1σ

uncertainties including errors in the J-parameter. Inverse isochron (correlation) diagram with $^{36}Ar/^{40}Ar$ vs. $^{39}Ar/^{40}Ar$ (see text for explanation). Grey ellipses are excluded from isochron regression (York, 1969 and York et al., 2005), MSWD stands for Mean Squares of Weighted Deviates.

Figure 09: A) Sketch locating the isotopic (yellow) and biostratigraphic (blue) data for all dredges along the platform flanks. The terraces identified on the platform flanks from morphological data after Courgeon et al., 2016 are indicated by blue quartering. B) Location map of dredges. C) Vertical movements inferred from dredge data.

Figure 10a: From top to bottom: Isochron maps of the respective top of the acoustic basement, and tops of sequences S1 and S2. Iso-contours every 100 ms twtt. Location of the Ptolémée seismic survey is superimposed on each map.
Figure 10b: From top to bottom: isochore and isopach maps of the respective mega-sequences S1 to S3 (increasing age order), and estimates of their respective associated volumes. Velocity for time-depth conversion: 2000 m/s. Iso-contours every 50 m. Location of the Ptolémée seismic survey is superimposed on each map.

Figure 11: 3D view of the evolution of the Glorieuses seamount and adjacent basins over the last 62 Ma. Paleo-topographies are calculated and re-drawn at 62 Ma, 35 Ma, 15 Ma and present-day. .

Figure 12: Results of this study placed in a chronostatigraphic framework and correlated to a compilation of the main geological events that could have impacted the stratigraphic record. The correlation of our observations to global and/or regional events (climatic and hydrodynamic changes, magmatism pulses, timing of uplifts) and to stratigraphic records in the surrounding areas suggest a long-term evolution for the Glorieuses stratigraphy including triggering factors. See the text for further explanation. Abb.: Pl: Pliocene, P:Pleistocene, Pia:Piacenzian, Gel: Gelasian; PD: Present-day; Comol: Comoledo islands, Ald: Aldabra, Faq: Faqhar. Compilation of existing data are (i) from Miller et al., 2008 for sea-level changes, (ii) from Zachos et al., 2001 for climate, (iii) from Reeves et al, 2014; Klimke et al., 2016; Thompson et al., 2019 (among others) for kinematics, (iv) from Hajash and Armstrong 1972; Montaggioni and Nougier 1981; Emerick and Duncan, 1982, 1983; Plummer, 1995; Storey et al., 1997; Rasamimanana et al., 1998; Class et al., 1998; Nougier et al. 1986; Debeuf, 2004; Nougier *et al.*, 2006; Bardintzeff et al., 2010 ; and Michon et al., 2016 for magmatism, (v) from Walford et al., 2005; Said et al., 2015, Castelino et al., 2015; Delaunay, 2018 (among others) for tectonics, (vi) from Martin et al., 1982; Townsend et al, 2010; Ali & Huber, 2010; Breitzke et al., 2017; Lanci et al., 2019 for hydrodynamics, (vii) from Simpson et al., 1974; Lort et al., 1979 ; Mougenot et al., 1986; Coffin & Rabinowitz, 1988; 1992;

Salman & Abdula, 1995; Franke et al., 2015 for stratigraphic record. See the text for more explanation and references.

Table 01: Results of isotopic and bio-stratigraphic analyses for dredge data. The ages provided by the two methods are consistent across all samples. Also see Figure 10 which spatially locates these results along the flank of the platform.

SAMPLES	DEPTHS	87Sr/86Sr	1sigma error	Age (Ma)	+ /- (Ma)	Minimum 87Sr/86Sr	Maximum Age (Ma)	+ /- (Ma)	Maximum 87Sr/86Sr	Minimum Age (Ma)	+ /- (Ma)
DW4819A	728-722 m	0.708919	0.000003	**8.89**	**0.33**	0.708916	9.03	**0.31**	0.708922	8.75	**0.35**
			>	8.56	0.33	>	8.72	0.31	>	8.37	0.38
			<	9.21	0.32	<	9.33	0.30	<	9.07	0.32
DW4819B	728-722 m										
DW4809A	301-293 m	0.708903	0.000003	**9.52**	**0.22**	0.708900	9.61	**0.20**	0.708906	9.43	**0.23**
			>	9.28	0.24	>	9.39	0.22	>	9.17	0.26
			<	9.71	0.19	<	9.79	0.18	<	9.63	0.20
DW4815	898-1012 m	0.707783	0.000003	**34.65**	**0.34**	0.707780	34.80	**0.38**	0.707786	34.53	**0.30**
			>	34.37	0.28	>	34.46	0.34	>	34.29	0.24
			<	35.05	0.40	<	35.23	0.43	<	34.89	0.36
DW4814	694-733 m DW4814B	0.708954	0.000003	**7.03**	**0.15**	0.708951	7.14	**0.16**	0.708957	6.91	**0.14**
			>	6.90	0.1	>	7.00	0.1	>	6.79	0.1

					3			4			2
			<	7.20	0.17	<	7.32	0.18	<	7.07	0.16
DW4814	**694-733 m DW4814B**										
DN01	**750 m**			**61.52**	1.80						

Table 02: Sediment volume estimates from thickness maps of each of the identified sequences (S1, S2 and S3).

MICROFACIES	COMPONENTS (reworked foraminifera are in red)	DEPOSITIONAL ENVIRONMENTS	AGE BASED ON FIRST APPEARANCE, Planktonic Foraminiferal zones, Shallow benthic zones and letter stages after BouDagher-Fadel (2008) and BouDagher-Fadel (2015) relative to the biostratigraphical time scale (as defined by Gradstein et al., 2012).
Micritic packstone of planktonic foraminifera	*Orbulina suturalis, Globoquadrina dehiscens, Orbulina bilobata, Globigerinoides ruber, Globorotalia merotumida, Globigerinoides quadrilobatus, Globigerinoides spp., Globorotalia menardii, Globigerinoides trilobus, Orbulina universa, Amphistegina spp., Elphidium sp., Dentoglobigerina altispira,*	Outer neritic	**LATE MIOCENE, N17b-N18, 7.2-5.3Ma**
Micritic packstone of planktonic foraminifera	*Orbulina suturalis, Globigerinoides ruber, Globoquadrina dehiscens, Paragloborotalia sp., Globorotalia plesiotumida, Sphaeroidinellopsis subdehiscens, Orbulina suturalis, Globigerinoides quadrilobatus, Globigerinoides spp.,, Dentoglobigerina altispira, Carpenteria sp., Globorotalia merotumida, Pulleniatina primalis, Neogloboquadrina acostaensis, Globorotalia inflata, Bolivina sp., Halimeda spp., dasyclad spp., rodophyte spp.*	Outer neritic	**LATE MIOCENE, N17b- N18, 7.2-5.3Ma**
Barren, no sediments in the section			
Micritic/sparitic packstone of algae and foraminifera	*Daviesina sp., Discocyclina spp., Neorotalia sp., small miliolids, Amphistegina spp., Textularia spp., Borelis sp., Paragloborotalia nana, Distichoplax biseralis, gastropod spp., echinoid spp., dasyclad spp., coral spp., rodophyte spp., Halimeda spp.*	Shallow water reefal environment with low to moderate energy	**LATE EOCENE, P15-P17, 38-33.9Ma**

Sparitic wackestone of algae and benthic foraminifera. Planktonic foraminifera are in micritic patches.	*Amphistegina spp., Neorotalia sp., Miogypsinodella pillaria, Alveolinella praequoyi, Globigerinoides quadrilobarus, Globorotalia merotumida, rodophyte spp., echinoid spp.*	Inner neritic with reworking of shallow reefal deposits.	**LATE MIOCENE, N16b-N18, 9-5.3Ma (reworked Early Miocene larger benthic foraminifera)**
Sparitic wackestone of algae and benthic foraminifera. Planktonic foraminifera are in micritic patches.	*Operculinella sp., Sphaerogypsina sp., Amphistegina spp., Miogypsina sp., Miogypsinodella pillaria, Sphaeroidinellopsis subdehiscens, Orbulina suturalis, Globigerinoides quadrilobatus, Globigerinoides spp., Prosphaeroidinella disjuncta, Orbulina universa, Sphaeroidinellopsis seminulina, Globorotalia menardii, Bulimina sp., gastropod spp., rodophyte spp.*	Inner neritic with reworking of shallow reefal deposits.	**The planktonic foraminifera assemblages is N13-N19, but not older than N16b or younger than N18, 9-5.3Ma, taking into account DW4814B. (reworked Early Miocene larger benthic foraminifera)**
Coralgal boundstone with pockets of Large benthic foraminifera packstone	*Red algae, large benthic foraminifera, coral, encrusting foraminifera, Bryozoans, Echinoids, Bivalves, Gastropods, Small benthic foraminifera, planktonic foraminifera*	Shallow-water tropical platform	**P3-P5a, 61.6–56.0 Ma, Selandian-Thanetian (Paleocene)**

Conflict of Interest

We confirm that we have no conflicts of interest related to this research, this work is original to its form and has not been published elsewhere, nor is under consideration for publication elsewhere.

Highlights

- The Glorieuses volcanic seamount emerged from two successive Late Cretaceous magmatic pulse(s).
- At least two potential uplift phases are recognized during the Tertiary.
- Basinal sedimentation recorded an abrupt change in Late Eocene times.
- Sediment export from platform to deep basin is strongly enhanced after Mid-Miocene
- History of Glorieuses seamount linked to the SSE-NNW Madagascar-Seychelles alignment.